Am J Transl Res 2024;16(10):5829-5845
www.ajtr.org /ISSN:1943-8141/AJTR0156998

Original Article

Zhi Zhu Ma Ren pill relieves constipation in mice through endoplasmic reticulum stress-mediated apoptosis

Yong Wen[1*], Yu Zhan[2,3*], Jun Li[1], Ling Xu[4], Chengzi Huang[1], Rong Wu[5], Xuegui Tang[6]

[1]Department of Traditional Chinese Medicine, The Affiliated Hospital of Southwest Medical University, Luzhou 646000, Sichuan, China; [2]Department of Clinical Medicine, Hospital of Chengdu University of Traditional Chinese Medicine, Chengdu 610000, Sichuan, China; [3]Department of Anal and Intestine Surgery, Chengdu First People's Hospital, Chengdu 610000, Sichuan, China; [4]Department of General Surgery, Hospital of Luzhou Traditional Chinese Medicine, Luzhou 646000, Sichuan, China; [5]Department of Clinical Medicine, Hospital of Chengdu University of Traditional Chinese Medicine, Chengdu 610000, Sichuan, China; [6]Department of Integrated Traditional and Western Medicine Anorectal, Affiliated Hospital of North Sichuan Medical College, Nanchong 637000, Sichuan, China. [*]Equal contributors.

Received April 3, 2024; Accepted September 22, 2024; Epub October 15, 2024; Published October 30, 2024

Abstract: Purpose: This study explores the detailed effects and mechanisms of Zhi Zhu Ma Ren Pill (ZZMRP) on constipation. Methods: Mouse constipation was induced by using loperamide (Lop). The effects and mechanisms of ZZMRP on constipation were addressed by various methods including charcoal meals, hematoxylin and eosin (H&E) staining, immunohistochemistry, enzyme-linked immunosorbent assay (ELISA), terminal deoxynucleotidyl transferase deoxyuridine triphosphate (dUTP) nick end labelling (TUNEL), transmission electron microscopy, and western blot experiments. Results: Lop-treated mice exhibited delayed transit and reduced ink progradation rates after charcoal meal administration. H&E staining confirmed severe pathologic symptoms in these mice. Additionally, a decline in interstitial Cajal cells (ICCs) was observed in Lop-treated mice, accompanied by reduced concentrations of 5-hydroxytryptamine (5-HT), acetylcholinesterase (AchE), substance P (SP), and vasoactive intestinal peptide (VIP), coupled with an elevated concentration of nitric oxide synthase (NOS). However, ZZMRP treatment markedly ameliorated these changes. In addition, ZZMRP introduction significantly reversed the Lop-induced enhancement in apoptosis rate, endoplasmic reticulum (ER) stress, and levels of proapoptotic proteins and ER stress proteins, and the decrease in the expression of antiapoptotic proteins. These effects were further confirmed with the use of 4-phenylbutyrate (4-PBA), which also reversed the changes in apoptosis rate and protein levels. Conclusion: ZZMRP alleviates constipation primarily through modulating ER stress-mediated apoptosis in Lop-treated mice, suggesting its use as a therapeutic agent for constipation.

Keywords: Constipation, Zhi Zhu Ma Ren pill, apoptosis, endoplasmic reticulum stress, mechanism

Introduction

Constipation is one of the most common chronic gastrointestinal disorders that influences individuals of all ages and both genders. It is characterized by infrequent or difficult defecation, incomplete evacuation, and hard stools [1]. Approximately 16% of adults worldwide suffer from constipation, leading to significant medical care costs annually [2]. Importantly, due to environmental and psychological stressors, the prevalence of constipation exceeds 20% in certain Asian populations [3]. Moreover, severe constipation can lead to complications such as retentive faecal incontinence, mental problems, and lower quality of life [4]. Additionally, constipation in females is related to obesity and hormonal diseases [5]. Despite various strategies have been applied for different degrees of constipation, including laxatives [6], biofeedback therapy [7], dietary fibre [8] and surgery [9] in clinical practice, the effectiveness and potential side effects of these interventions are still unclear. Therefore, effective agents are urgently needed for the development of clinical treatments for constipation. Consequently, there is an urgent need for the development of effective and safe therapeutic agents for constipation.

https://doi.org/10.62347/YLIE1988

Traditional Chinese medicine (TCM) is frequently utilized for the treatment of constipation, with remedies such as *Rhei Radix et Rhizoma* (rhubarb) [10], modified RunChang-Tang [11] and Dahuang-Gancao decoction [12]. "Zhi Zhu Ma Ren Pill" (ZZMRP), a proprietary TCM formulation, contains *Aurantii Fructus Immaturus* (Zhishi), *Atractylodis Macrocephalae Rhizoma* (Baizhu), *Fructus Cannabis* (Huomaren), *Paeonia lactiflora* (Baishao) and *Radix Asteris* (Zi-wan). These ingredients have been revealed to exert improved effects on intestinal diseases, including constipation. For example, Zhishi volatile oil has been used to treat slow transit constipation in a network pharmacology study [13]. The combination of Zhishi and Baizhu exhibits a positive effect on slow transit constipation [14]. In addition, Baizhu and Huomaren are known to alleviate symptoms of constipation, abdominal fullness, and dyschezia [15]. Furthermore, the ethanol extracts of Huomaren display laxative properties that affect Cl^- and Na^+ movement in intestinal epithelial cells [16]. Total glucosides from Baishao alleviate Sjögren's syndrome-induced intestinal inflammation and constipation [17]. Significantly, our recent study has reported the mechanistic prediction of ZZMRP in the treatment of constipation using network pharmacology and molecular docking [18]. While our findings revealed the likely therapeutic effects of ZZMRP on constipation, further experimental validation is necessary. Hence, this study focuses on the effects and mechanisms of ZZMRP in treating constipation.

Multiple mechanisms contribute to the pathogenesis of constipation. Our previous mechanistic prediction of ZZMRP for treating constipation identified 18 key targets, including tumour protein p53, RAC-alpha serine/threonine-protein kinase, JUN, and caspase-3. Additionally, several signalling pathways are related to the treatment of constipation by ZZMRP, such as mitogen-activated protein kinase and phosphoinositide 3-kinase/protein kinase B (PI3K-Akt) signalling pathways, along with tumour necrosis factor pathway [18]. Notably, key targets like p53 and caspase-3, which play an important role in apoptosis, suggest that apoptosis may be a crucial signalling pathway in the treatment of constipation by ZZMRP. Research has underscored the pivotal role of apoptosis in the progression of constipation, where inhibition of apoptosis is an alternative strategy for the treatment of constipation [19]. Furthermore, endoplasmic reticulum (ER) stress is also a vital mechanism underlying constipation. The ER is responsible for protein synthesis, post-translational modification, processing, folding, and transportation. Maintaining normal ER function is indispensable for the sustainability of cellular homeostasis, particularly in specialized secretory cells such as chondrocytes, which are responsible for the synthesis and turnover of extracellular matrix macromolecules [20]. Observations in constipated mice reveal activation of ER stress proteins and alterations of ER structure [21], and suppression of ER stress exhibits laxative effects in constipation rats [22]. Therefore, agents that mitigate apoptosis and ER stress may be candidates for the treatment of constipation.

In the current study, we comprehensively examined the effects and underlying mechanism of ZZMRP on constipation in loperamide (Lop)-induced mice. Initially, we evaluated the overall impact of ZZMRP on constipated mice. Subsequently, we specifically investigated the effect of ZZMRP on apoptosis and ER stress in Lop-treated mice.

Materials and methods

Herbal materials and drug preparation

Aurantii Fructus Immaturus (Zhishi), *Atractylodis Macrocephalae Rhizoma* (Baizhu), *Fructus Cannabis* (Huomaren), *Paeonia lactiflora* (Baishao) and *Radix Asteris* (Zi-wan) were sourced from Sichuan Traditional Chinese Medicine Decoction Piece Co., Ltd. (Sichuan, China), with the respective production batch numbers being 220221, 220722, 221227, 211123, and 201229.

The preparation involved combining 15 g Zhishi, 60 g Baizhu, 15 g Huomaren, 15 g Baishao and 10 g Zi-wan in water at a ratio of 1:10 (w/v). This mixture was soaked in water for 20 minutes before boiling for 30 min and subsequently filtered. The residue was then reboiled at a ratio of 8:1 (v/w) for 20 minutes. The two extracts were mixed, refiltered, and concentrated to a final concentration of 1 g/mL to produce ZZMRP decoction storage solution, which was stored at -20°C. Decomposed included DR1, containing Zhishi, Zi-wan and Baizhu, while DR2 included Huomaren and Baishao.

Metabolite extraction

100 mg of the samples (ZZMRP, DR1 and DR2) were added to 500 μL of extracted solution composed of 80% methanol with 10 μg/mL internal standard. After 30 s vortex, the samples were homogenized at 45 Hz for 4 min and sonicated for 1 hour in ice-water bath. After 1 hour at -40°C, the samples were centrifuged at 12,000 rpm (reactive centrifugal force (RCF) = 13,800 (×g), radius (R) = 8.6 cm) for 15 min at 4°C. The supernatant was carefully filtered through a 0.22 μm microporous membrane, with 50 μL from each sample pooled as quality control (QC) samples and stored at -80°C for subsequent ultra-high-performance liquid chromatography coupled to tandem mass spectrometry (UHPLC-MS) analysis.

Liquid chromatography-mass spectrometer mass spectrometer (LC-MS/MS) conditions

LC-MS/MS analysis was performed using an UHPLC system (Vanquish, Thermo Fisher Scientific) with a Waters UPLC BEH C18 column (1.7 μm 2.1×100 mm). The flow rate was maintained at 0.4 mL/min, and the injection volume was 5 μL. The mobile phase consisted of 0.1% formic acid in water (A) and 0.1% formic acid in acetonitrile (B). The multi-step linear elution gradient program was set as follows: from 0 to 3.5 minutes, 95-85% A; 3.5-6 minutes, 85-70% A; 6-6.5 minutes, 70-70% A; 6.5-12 minutes, 70-30% A; 12-12.5 minutes, 30-30% A; 12.5-18 minutes, 30-0% A; 18-25 minutes, 0-0% A; 25-26 minutes, 0-95% A; 26-30 minutes, 95-95% A.

An Orbitrap Exploris 120 mass spectrometer, controlled by Xcalibur software, was employed to obtain MS and MS/MS data in IDA mode. During each acquisition cycle, the mass range was from 100 to 1500, and the top four ions from every cycle were selected for further analysis. Operational settings included a sheath gas flow rate of 30 Arb, an auxiliary gas flow rate of 10 Arb, ion transfer tube temperature of 350°C, vaporizer temp of 350°C, full ms resolution of 60,000, MS/MS resolution of 15,000, collision energy of 16/32/48 in NCE mode, and a spray voltage of 5.5 kV for positive or -4 kV for negative mode.

Data processing and statistical analysis

Data processing was performed using Progenesis QI software (Waters, Manchester, U.K.) for LC-MS/MS data management and pathway analysis, generating a peak table that contains information on retention time, mass-to-charge ratio (m/z), and MS intensity of the ingredients in the sample. The raw data files from LC-MS/MS were uploaded to Progenesis QI for analysis.

The data were evaluated using principal component analysis (PCA) to visualize general clustering, outliers, or trends among the observations. Putative ingredients were identified by searching the exact molecular mass data from redundant m/z peaks against the online Kyoto Encyclopaedia of Genes and Genomes (KEGG) (http://www.kegg.jp/), Human Metabolome database (HMDB) (http://www.hmdb.ca/), Metlin (https://metlin.scripps.edu), Chemical Abstracts Service (CAS) (https://www.cas.org/), PubMed (http://www. ncbi.nlm.nih.gov/pubmed/), and chEMBL (https://www.ebi.ac.uk/chembl/) databases. Differential ingredients were visualized using volcano plots, and key pathways associated with these differences were analysed by KEGG.

Animals

Male Kunming mice (32-38 g) were provided by Chengdu Dashuo Laboratory Animal Co., Ltd. (Chengdu, China) and housed under specific pathogen-free (SPF) conditions. The environment was maintained with 40%-60% relative humidity and a 12 h/12 h ligh/dark cycle at 22°C. All procedures were strictly conducted following the Ethics Committee of North Sichuan Medical College (Approval number: NSMC2021-82) as well as the ARRIVE guidelines. The animal protocol was designed to minimize pain or discomfort to the animals.

Animal group and treatment

Forty-two male mice were randomly divided into seven groups (n = 6 each): control, Lop, Lop+ZZMRP, Lop+decomposed recipe (DR) 1, Lop+DR2, Lop+4-PBA and Lop+mosapride (Mos). Mice received 10 mg/kg of loperamide hydrochloride daily by gavage for 14 consecutive days [23]. Starting on the 8th day, mice were intragastrically administered with DR1, DR2, and ZZMRP 1 hour post-loperamide in the respective groups. Mice in the control and Lop groups received an equivalent volume of normal saline. In addition, mice in the Lop+Mos

group received 1.6 mg/kg of mosapride daily [24], and the Lop+4-PBA group were intragastrically administered 1 g/kg of 4-PBA 0.5 h prior to Lop administration [25] starting on the 8th day. Body weight was recorded every two days. After the final treatment, 24-hour faeces samples were collected for analysis. Daily health monitoring included observations of food intake, coat condition, activity status and survival. Mice showing inability to eat or drink, abnormal behavior, or signs of toxicity, pain, or distress, were removed from the study. At the end of the experiment, the mice were euthanized by inhaling excess isoflurane (R510-22, RWD, Shenzhen, China), followed by cervical dislocation to collect blood, colon tissues, and contents for subsequent measurement.

Quantification of intestinal transit rate

To assess intestinal motility, mice were intragastrically administered a charcoal meal (20 mL/kg, 3% activated charcoal in 0.5% aqueous methylcellulose) 30 minutes after the last treatment. Forty minutes later, the mice were euthanized and the intestinal transit rate was calculated as the travelled distance of activated charcoal in the intestine (cm) divided by the full length of the small intestine (cm) ×100%.

Haematoxylin and eosin (H&E) staining

Fixed colon tissues were embedded, sectioned (5 μm), and stained using a Haematoxylin and Eosin Staining Kit (C0105S, Beyotime). Images were captured under a light microscope (Olympus, Tokyo, Japan).

Immunohistochemistry assays

Fixed colon tissues were dehydrated with gradient concentrations of ethanol, embedded into paraffin (YA0011, Solarbio, Beijing, China), and sectioned at a thickness of 5 μm with an automatic microtome (E0972, Beyotime). After drying and deparaffinization, sections underwent antigen retrieval in citrate solution (pH 6.0, P0081, Beyotime) at 94°C for 15 min, blocked with 1% bull serum albumin (BSA) (ST2249, Beyotime) for half an hour, and incubated with primary antibodies against c-kit (ab231780, 1:500, Abcam, Cambridge, UK). After being incubated with the secondary antibody labelled with HRP (ab6721, 1:1000, Abcam), the sections were restained with haematoxylin (C0107, Beyotime), and visualized by a light microscope (Olympus).

Enzyme-linked immunosorbent assay (ELISA)

The blood samples were collected by enucleation of eyeball, allowed to stand at room temperature for 1 hour, and then centrifuged at 4000 g for 10 minutes to collect serum. The serum concentrations of acetylcholinesterase (AchE), vasoactive intestinal peptide (VIP), substance P (SP), nitric oxide synthase (NOS), and 5-hydroxytryptamine (5-HT) in colon tissues, were quantified using commercial ELISA kits according to manufacturer instructions.

Terminal deoxynucleotidyl transferase deoxyuridine triphosphate (dUTP) nick end labelling (TUNEL) detection

Apoptosis in colon tissues was detected using an *in situ* cell death detection kit with fluorescein (11684795910, Roche), following the operating instructions. Paraffin-embedded sections were dewaxed, rehydrated through graded ethanol, and treated with citrate antigen retrieval solution (P0083, Beyotime) for 8 min by using a microwave oven. After washing with PBS for three times with 5 min each time at room temperature, sections were incubated with TUNEL reaction mixtures for 1 hour at 37°C, restained with DAPI (P0131, Beyotime) for 10 minutes at room temperature, and imaged under a fluorescence microscope (Olympus). Each section was initially observed at 100× to rule out false positives, and the proportion of positive area of each panoramic image was calculated to determine the apoptosis.

Transmission electron microscopy

Colon tissues were fixed in 3% glutaraldehyde and 1% osmium tetroxide, sectioned using an ultramicrotome, and stained sequentially with 1% uranyl acetate and 0.5% lead citrate. Images were captured using a JEM-1400PLUS transmission electron microscope.

Western blot

Colon tissues were lysed with radio immunoprecipitation assay (RIPA) lysis buffer (P0013B, Beyotime) and protein concentrations were determined with a BCA Protein Assay Kit

(P0012S, Beyotime). Protein samples (20 μg) were separated using 10% sodium dodecyl sulfate-polyacrylamide gel electrophoresis (SDS-PAGE) and then transferred onto polyvinylidene fluoride (PVDF) membranes (IPVH00010, EMD Millipore, Billerica, MA, USA). The membranes were blocked in 5% skim milk powder (P0216, Beyotime) for 1 hour at room temperature, incubated overnight at 4°C with primary antibodies, followed by 1 hour of incubation with HRP-conjugated secondary antibodies (goat anti-rabbit IgG H&L, 1:20,000, ab6721, Abcam; goat anti-mouse IgG H&L, 1:10,000, ab6789, Abcam) at room temperature. The protein bands were visualized using a BeyoECL Plus kit (P0018S, Beyotime), and densitometry was examined using Image-ProPlus software (Media Cybernetics, Inc., Rockville, MD, USA). Relative protein expression was normalized to glyceraldehyde-3-phosphate dehydrogenase (GAPDH). The primary antibodies used included anti-Bcl-2 (1:2000, ab196495, Abcam), anti-Bax (1:5000, ab32503, Abcam), anti-cleaved-caspase-3 (1:5000, ab214430, Abcam), anti-cleaved-PARP (1:5000, ab32064, Abcam), anti-IRE1α (1:1000, ab37073, Abcam), anti-phosphorylated IRE1α (p-IRE1α) (1:2000, ab48187, Abcam), anti-TRAF2 (1:1000, ab2443-17, Abcam), anti-PERK (1:1000, ab229912, Abcam), anti-p-PERK (1:5000, ab192591, Abcam), anti-eIF2α (1:3000, ab155649, Abcam), anti-p-eIF2α (1:5000, ab32157, Abcam), anti-CHOP (1:1000, ab11419, Abcam), anti-ATF6 (1:1000, ab37149, Abcam), anti-GRP78 (1:1000, ab21685, Abcam) and anti-β-actin (1:10,000).

Statistical analysis

Statistical analysis was carried out using SPSS 20.0 software (IBM Corp., Armonk, NY, USA). All data are presented as the mean ± standard deviation. One-way analysis of variance was utilized to analyse the differences among multiple groups. The differences were considered significant when $P<0.05$.

Results

Analysis of the ingredients of ZZMRP

The ingredients of ZZMRP were analyzed by LC-MS/MS, revealing that there were 1948, 1782 and 1971 ingredients in DR1, DR2 and ZZMRP, respectively. Detailed listings of positive and negative ingredients of DR1, DR2 and ZZMRP are shown in Figures S1, S2, S3, S4, S5 and S6, with the top 20 ingredients of DR1, DR2 and ZZMRP in Table S1.

A total of 215 distinct ingredients were identified in ZZMRP compared to DR1, including 24 upregulated ingredients and 191 downregulated ingredients (**Figure 1A**). Additionally, a total of 1358 ingredients were identified in ZZMRP compared to DR2, with 501 upregulated and 857 downregulated ingredients (**Figure 1B**). Differential ingredients were subjected to KEGG enrichment analysis, revealing that differential ingredients between ZZMRP and DR1 were involved in several pathways: the mammalian target of the rapamycin (mTOR) signaling pathway, peroxisome proliferator-activated receptor (PPAR) signaling pathway, forkhead box O (FoxO) signaling pathway, and cyclic guanosine monophosphate (cGMP)-protein kinase G (PKG) signaling pathway (**Figure 1C**), while the differential ingredients between ZZMRP and DR2 were associated with FoxO signaling pathway, protein digestion and absorption, and nucleotide metabolism (**Figure 1D**).

ZZMRP improved constipation in Lop-induced mice

The mouse constipation model was established by using Lop, followed by gavaging with a charcoal meal to evaluate intestinal motility. Lop treatment significantly delayed the time to the first black bowel movement and reduced the ink progression rate in the mice (**Figure 2A** and **2B**). Histologic examination revealed mucosal atrophy, necrosis and exfoliation, widened lamina propria, inflammatory cell infiltration, gland atrophy in large intestine, sparse goblet cells, and thickening of the inner ring (**Figure 2C**). In addition, IHC results showed a reduced number of interstitial cells of Cajal (ICCs) and disappearance of intermuscular ICCs in Lop-induced mice (**Figure 3A**). Furthermore, there was a significant decrease in 5-HT levels in colon tissues and serum concentrations of AchE, SP and VIP, along with an increase in NOS in Lop-induced mice (**Figure 3B-F**). Taken together, these results indicated that a successful constipation model was constructed in mice, that could be used in subsequent studies.

However, treatment with ZZMRP, DR1 and Mos notably decreased the time to first black bowel movement. ZZMRP and Mos markedly reduced

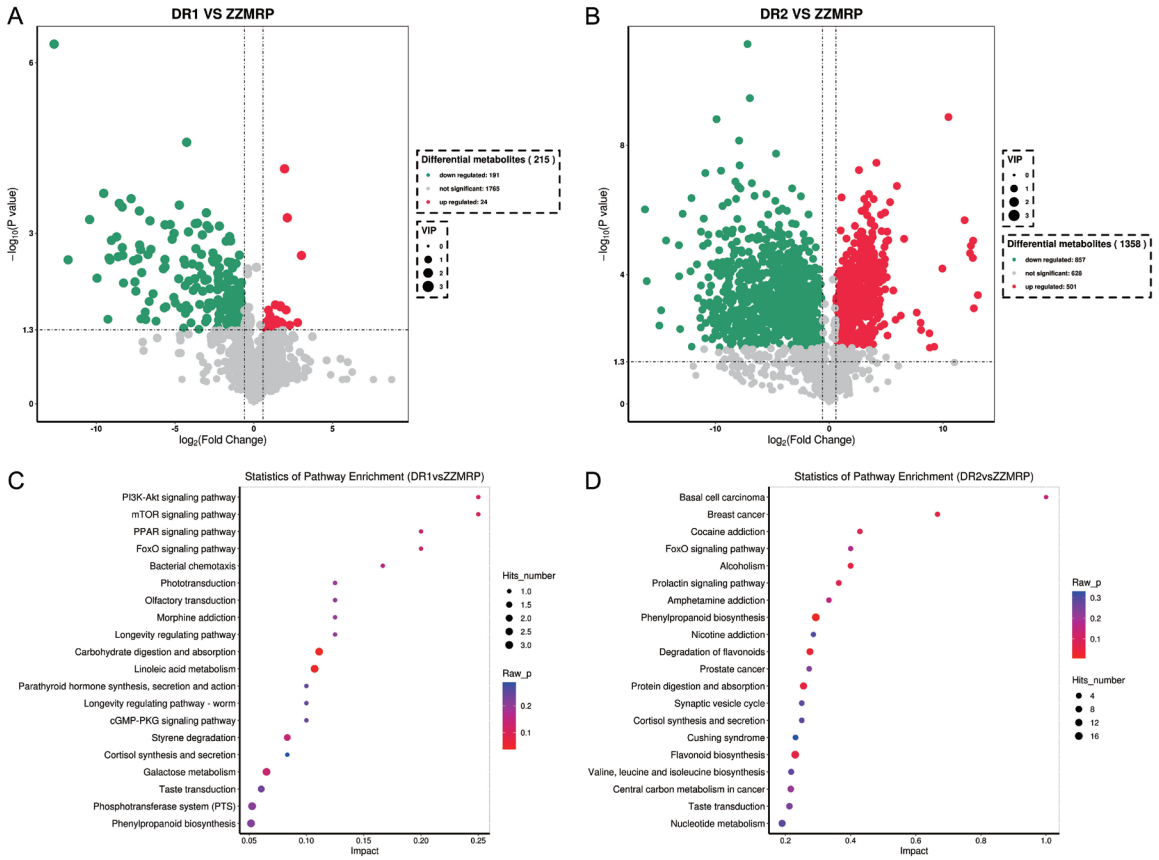

Figure 1. Differential ingredients and key pathways of ZZMRP, DR1, and DR2 analysis. A. Differential ingredients between ZZMRP and DR1. B. Differential ingredients between ZZMRP and DR2. C. KEGG enrichment analysis of differential ingredients between ZZMRP and DR1. D. KEGG enrichment analysis of differential ingredients between ZZMRP and DR2.

the ink progradation rate in Lop-induced mice (**Figure 2A** and **2B**). ZZMRP treatment obviously ameliorated pathologic symptoms (**Figure 2C**) and increased the number of intermuscular ICCs (**Figure 3A**). Additionally, ZZMRP, DR2 and Mos treatment significantly increased the Lop-induced concentration of 5-HT in colon tissues and the serum concentrations of SP while observably decreasing the serum NOS concentrations. The decrease in the serum AchE and VIP in Lop-induced mice was significantly reversed by ZZMRP and Mos treatments (**Figure 3B-F**), demonstrating the effectiveness of ZZMRP in improving constipation in Lop-induced mice.

ZZMRP attenuated apoptosis in Lop-induced mice

To assess the effect of ZZMRP on apoptosis, colonic tissues from Lop-induced mice were subjected to TUNEL and western blot assays. The results indicated that the apoptosis rate was significantly increased in Lop-treated mice, but it was substantially reduced following treatment ZZMRP, DR1, DR2 and Mos (**Figure 4A** and **4B**). Additionally, the relative protein levels of Bcl-2 were notably diminished, whereas those of Bax, cleaved caspase-3, and cleaved PARP were markedly elevated in Lop-treated mice (**Figure 4C-G**). However, administration of ZZMRP, DR1, DR2, and Mos reversed the expression of these proteins (**Figure 4C-G**), thus demonstrating that ZZMRP alleviates apoptosis in Lop-induced mice.

ZZMRP mitigated ER stress in Lop-induced mice

Additionally, the role of ZZMRP on ER stress was evaluated in Lop-induced mice. Control mice exhibited abundant rough endoplasmic reticulum ribosomes around the nucleus, a clear bilayer membrane structure, and a normally spaced endoplasmic reticulum pool. In contrast, Lop-treated mice displayed signifi-

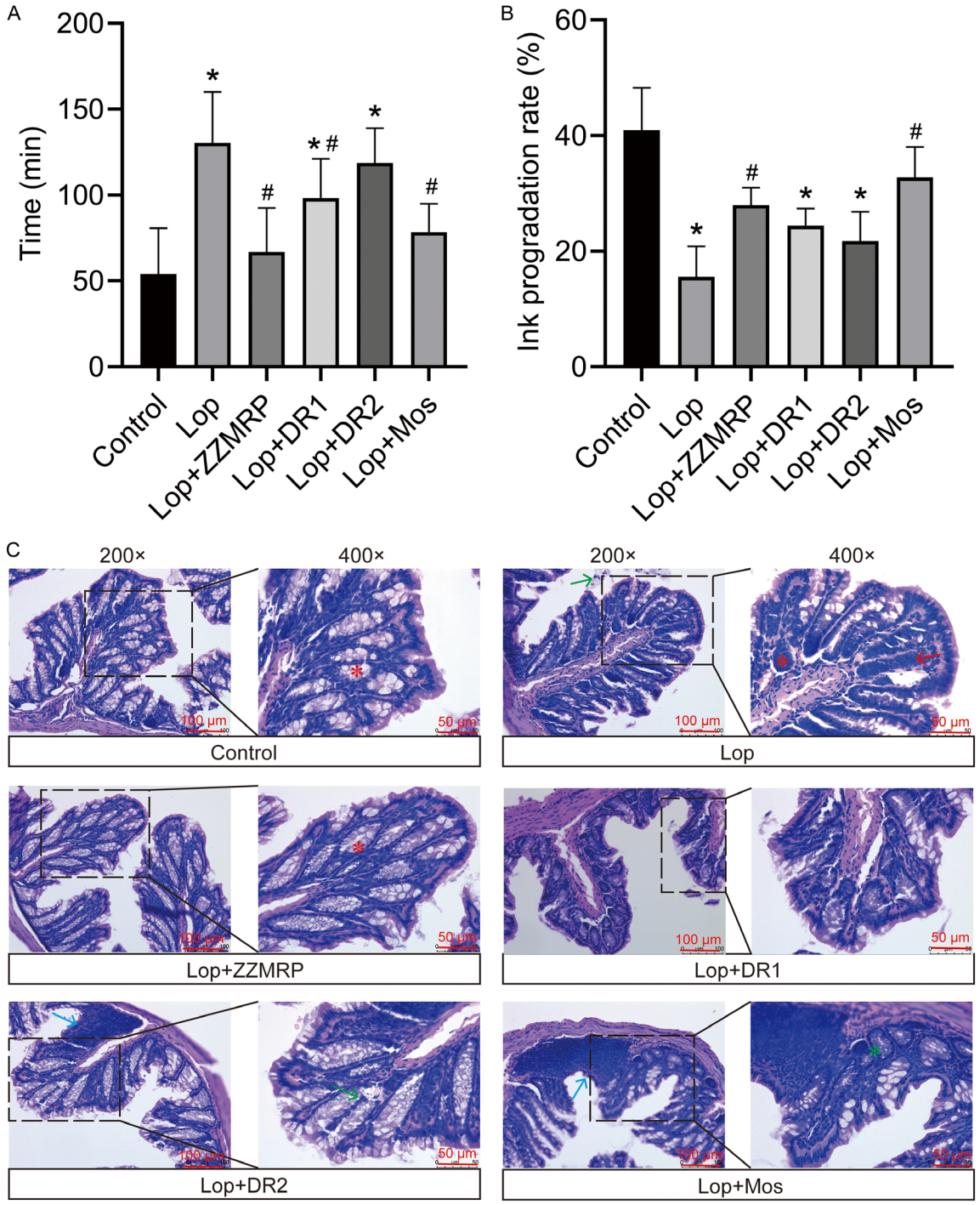

Figure 2. ZZMRP improved intestinal motility and pathologic symptoms in Lop-induced mice. A. Time to the first black bowel movement. B. The ink progradation rate. C. H&E staining of colon tissues highlight histological changes: Red asterisks indicate abundant and well-arranged goblet cells; red arrows point to inflammatory cell infiltration; blue arrows denote submucosal lymphocyte hyperplasia; green arrows highlight partial colonic mucosal epithelial cell necrosis; green asterisks mark partial colorectal gland atrophy. Significance indicators: **P*<0.05 *vs.* Control; #*P*<0.05 *vs.* Lop.

cantly reduced rough endoplasmic reticulum, detached ribosomes, and varied numbers of vacuoles or electron densities in the mitochondrial matrix (**Figure 5A**). Western blotting further revealed that the relative protein levels of p-IRE1α/IRE1α, TRAF2, p-PERK/PERK,

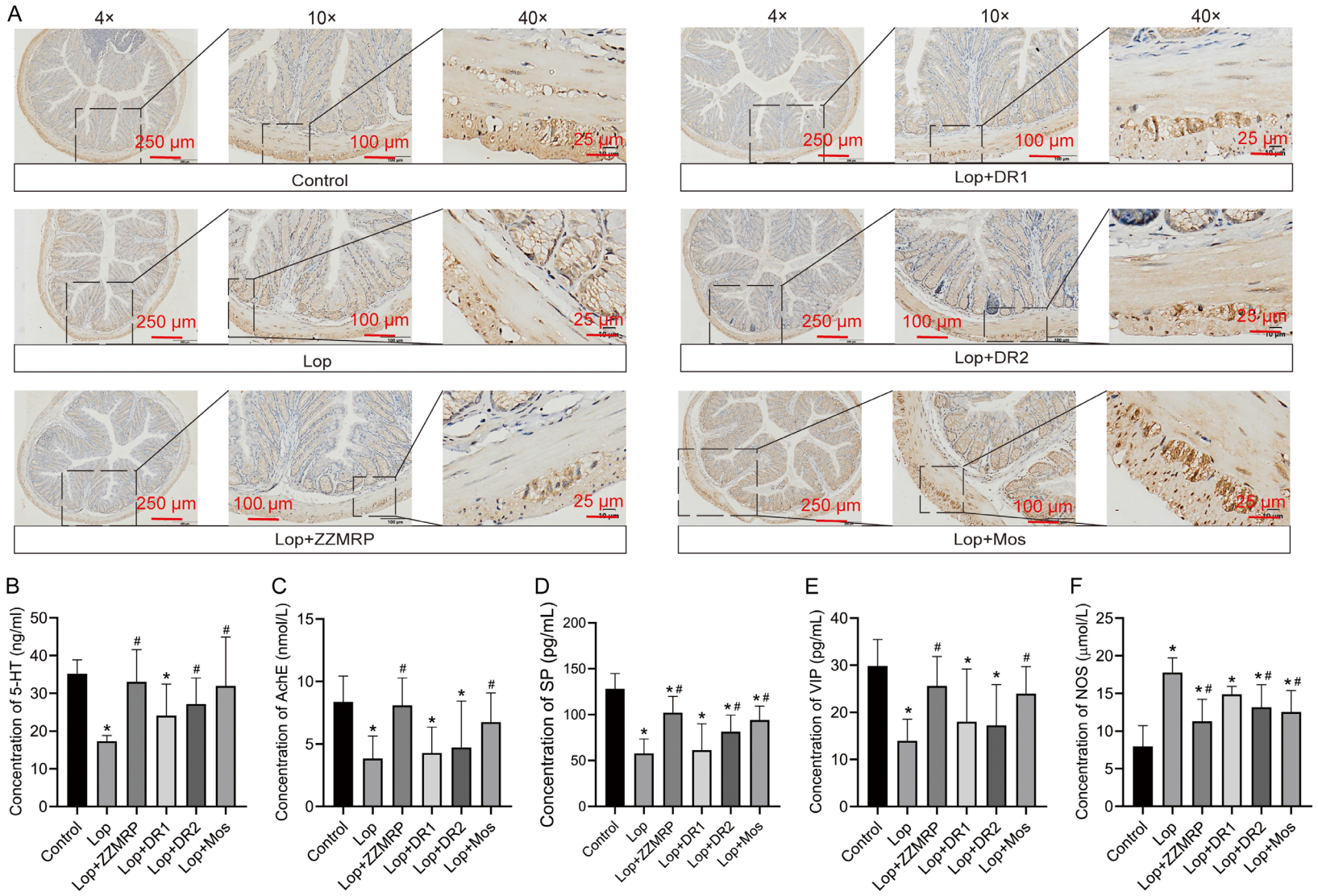

Figure 3. ZZMRP ameliorated the level of ICCs and gastrointestinal tract hormones in Lop-induced mice. A. Examination of ICCs expression by IHC assay. B-F. The concentrations of 5-HT, AChE, SP, VIP, and NOS were measured by ELISA kits. Significance indicators: **P*<0.05 *vs.* Control; #*P*<0.05 *vs.* Lop.

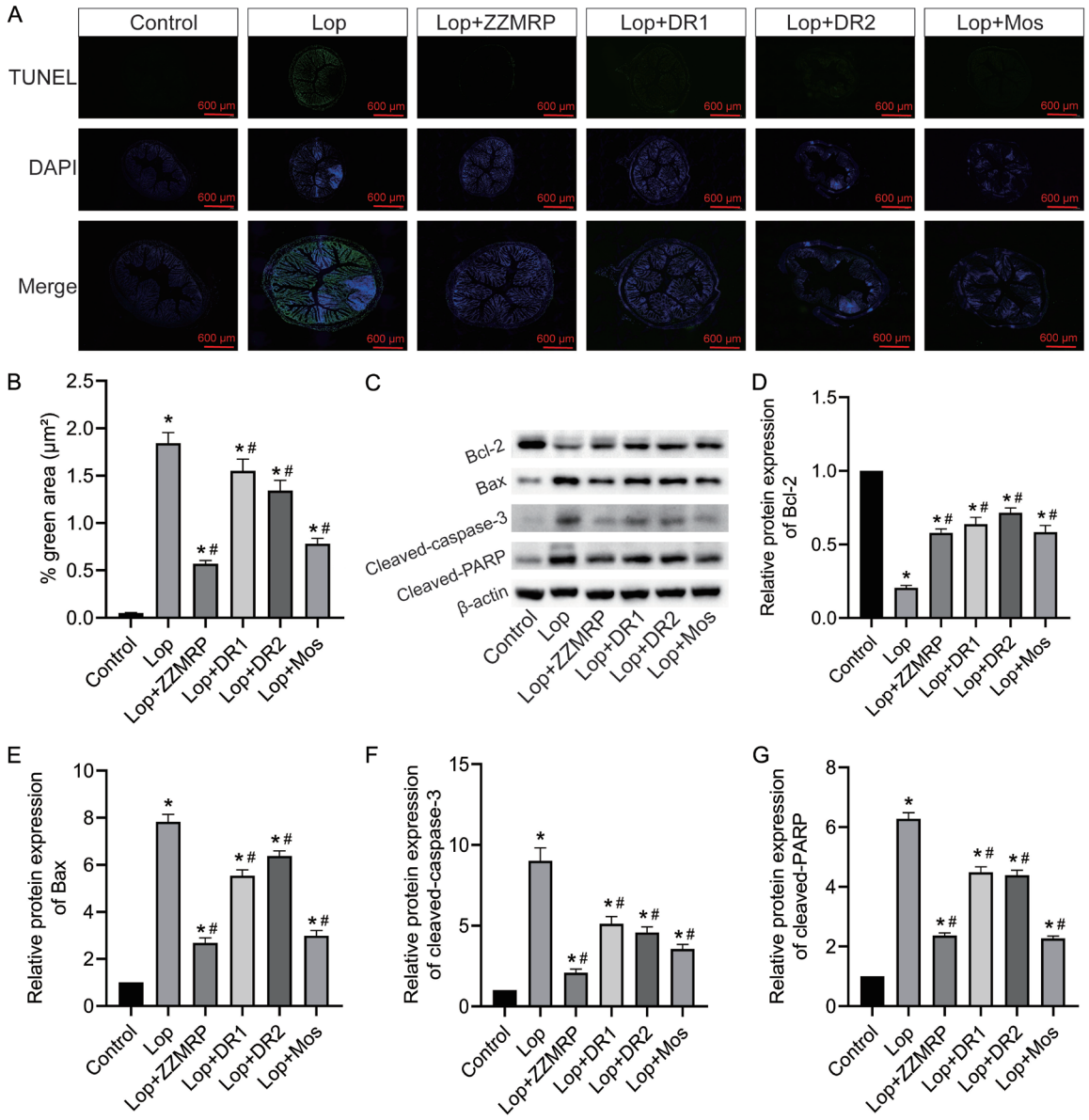

Figure 4. ZZMRP repressed apoptosis in Lop-induced mice. A and B. The apoptosis of colon tissues was assessed by TUNEL assay. C-G. The relative protein levels of Bcl-2, Bax, cleaved caspase-3, and cleaved PARP were detected by western blot. The results are displayed after normalization to β-actin. Significance indicators: *P<0.05 *vs.* Control; #P<0.05 *vs.* Lop.

p-eIF2α/EIF2α, p-CHOP/CHOP, ATF6, and GRP78 were significantly increased in Lop-induced mice (**Figure 5B-J**). These levels were neutralized by the introduction of ZZMRP and Mos (**Figure 5B-J**). Overall, ZZMRP improved ER stress in Lop-induced mice.

ZZMRP relieves apoptosis by mitigating ER stress in Lop-induced mice

To further elucidate the mechanism behind the ameliorative effect of ZZMRP on constipation, mice were administered with 4-PBA. Treatment with 4-PBA markedly improved the symptoms caused by ER stress in Lop-treated mice, similar to the effects observed with ZZMRP and Mos treatment (**Figure 6A**). Consistently, both the application of 4-PBA and treatment with ZZMRP and Mos prominently decreased the Lop-triggered relative protein levels of p-IRE1α/IRE1α, TRAF2, p-PERK/PERK, p-eIF2α/EIF2α, p-CHOP/CHOP, ATF6, and GRP78 (**Figure 6B-J**). All these data indicated that 4-PBA effectively repressed ER stress, thereby decreasing the

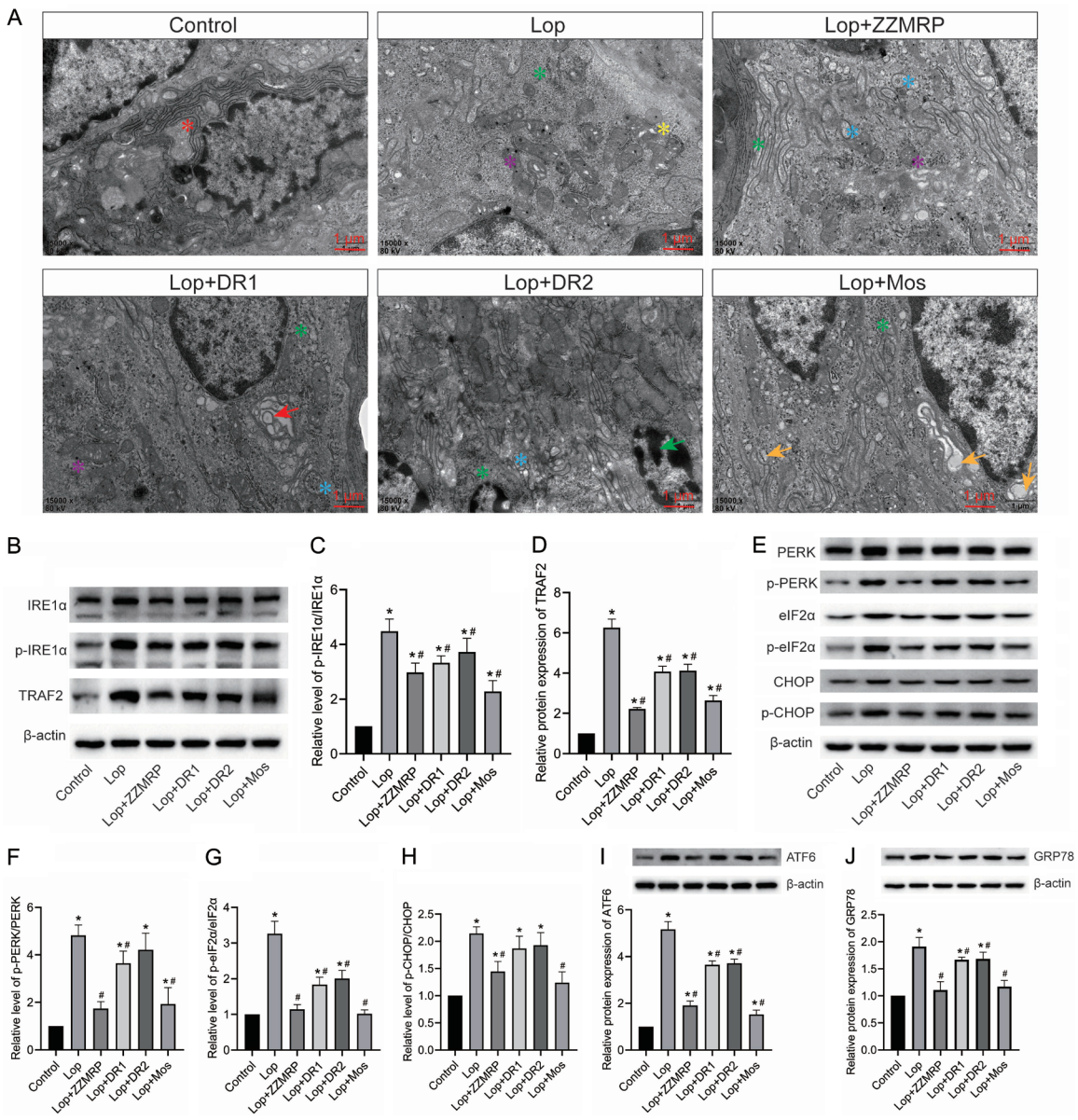

Figure 5. ZZMRP alleviated ER stress in Lop-induced mice. A. ER stress was assessed by transmission electron microscopy: Red asterisk indicates normal rough-faced endoplasmic reticulum ribosomes; green asterisk for ribosome shedding; yellow asterisk for vacuoles of varying numbers; purple asterisk for electron-dense particles; blue asterisk for the slightly dilated slippery surface endoplasmic reticulum cell containing fine and granular contents; red arrows for isolation bubbles in the endoplasmic reticulum pool; green arrows for nuclear nucleoplasmic concentration marginalization; yellow arrows for the expanded endoplasmic reticulum and bubble-like structures of various sizes. B-D. Relative protein expression of p-IRE1α, IRE1α, and TRAF2 was assessed by western blotting and normalized to β-actin. E-H. Relative protein levels of p-PERK, PERK, p-eIF2α, EIF2α, p-CHOP and CHOP was examined by western blotting and normalized to β-actin. I. Relative protein expression of ATF6 was determined by western blotting and normalized to β-actin. J. Relative protein level of GRP78 was assessed by western blotting and normalized to β-actin. Significance indicators: **P*<0.05 *vs.* Control; #*P*<0.05 *vs.* Lop.

Lop-induced apoptosis rate in mice (**Figure 7A** and **7B**). Administration of 4-PBA significantly recovered the Lop-induced relative protein level of Bcl-2 and counteracted the elevated levels of Bax, cleaved caspase-3, and cleaved PARP (**Figure 7C-G**). Collectively this shows that ZZMRP inhibits apoptosis by mitigating ER stress in Lop-induced mice.

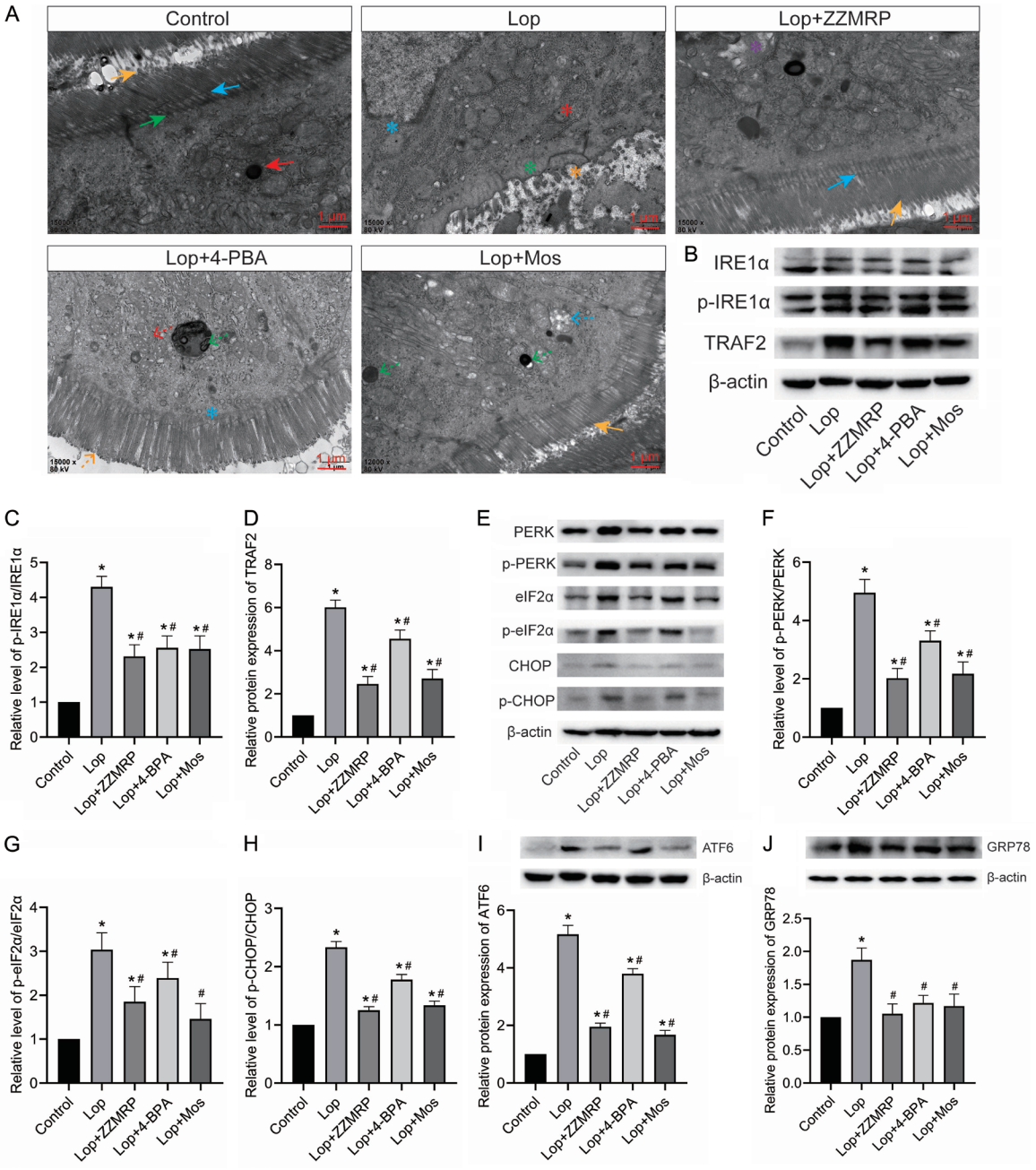

Figure 6. 4-PBA application effectively inhibited ER stress. A. ER stress was assessed by transmission electron microscopy: Yellow arrows show that the intestinal epithelial cells were neatly arranged with cell coats visible on the microvilli; green arrows show penetration deep into the axis filaments within the cytosolic terminal reticulum; blue arrows show a clear plasma membrane; blue asterisks show the defective nuclear membrane; red asterisks show electron-dense particles; green asterisks for the disappearance of the plasma membrane and axial filaments; yellow asterisks show sparse, broken and lysed intestinal epithelial cell microvilli; purple asterisks show hollow concentric circular lamellar endoplasmic reticulum in the cytoplasm; red dotted arrows show reduced rough endoplasmic reticulum; green dotted arrows show increased mitochondrial matrix electron density; yellow dotted arrows show that intestinal epithelial cell microvilli were not tightly arranged; blue dotted arrows show that the mitochondria were swollen and vacuoles appeared within the stroma. B-D. Relative protein expression of p-IRE1α, IRE1α, and TRAF2 was detected by western blotting and normalized to β-actin. E-H. Relative protein level of p-PERK, PERK, p-eIF2α, EIF2α, p-CHOP and CHOP was examined by western blotting and normalized to β-actin. I. Relative protein expression of ATF6 was determined by western blotting and normalized to β-actin. J. Relative protein level of GRP78 was assessed by western blotting and normalized to β-actin. Significance indicators: **P*<0.05 *vs.* Control; #*P*<0.05 *vs.* Lop.

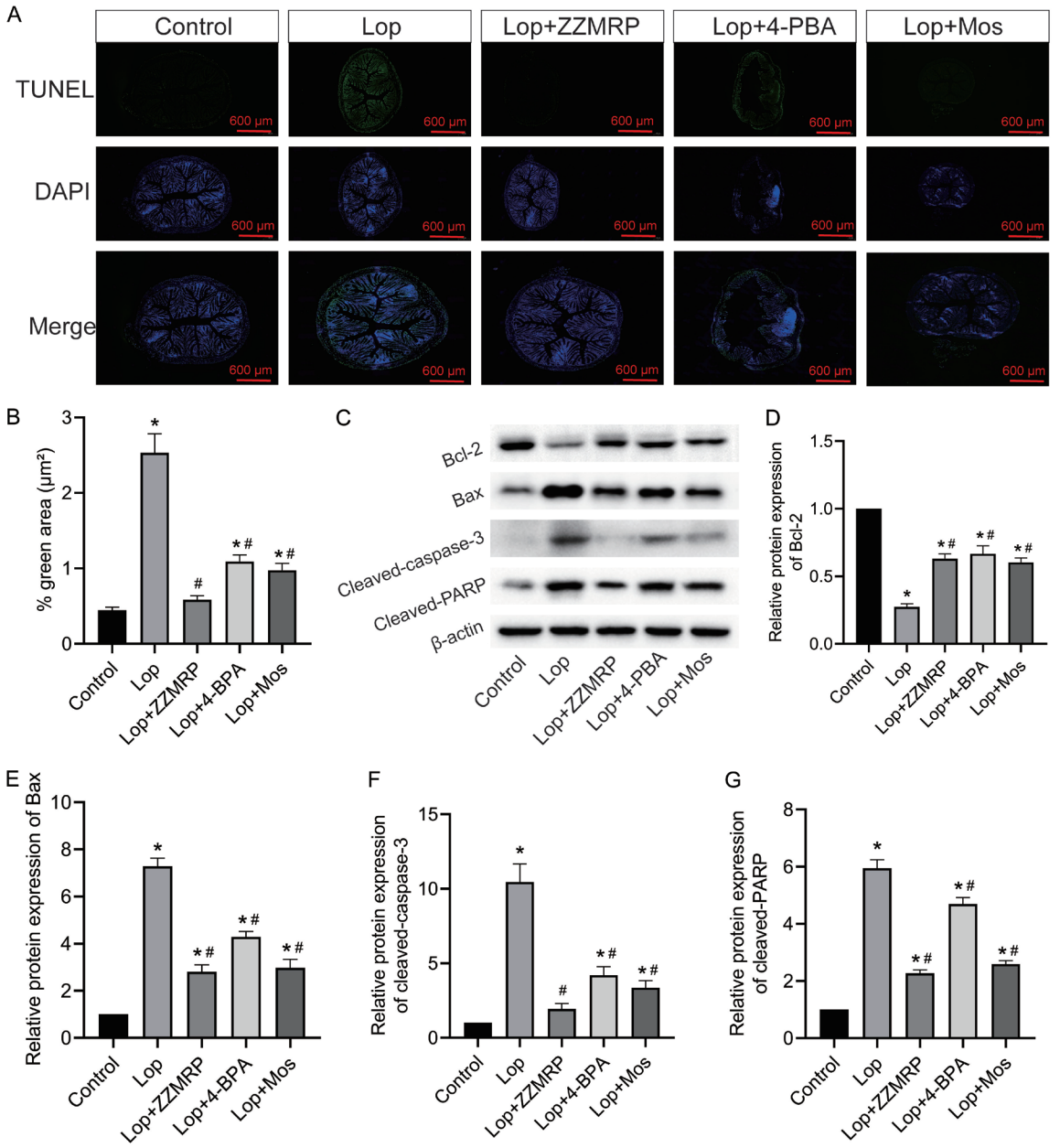

Figure 7. ZZMRP dampened apoptosis through ER stress in Lop-induced mice. A and B. The apoptosis of colon tissues was assessed by TUNEL assay. C-G. Relative protein levels of Bcl-2, Bax, cleaved caspase-3, and cleaved PARP were examined by western blotting, shown after normalization to β-actin. Significance indicators: **P*<0.05 *vs.* Control; #*P*<0.05 *vs.* Lop.

Discussion

In the current study, constipation was induced in mice by the application of Lop. Mice treated with Lop exhibited prolonged transit times and reduced ink progradation rates following the administration of charcoal meal. H&E staining confirmed severe pathologic symptoms in Lop-induced mice. Additionally, we observed reduced levels of ICCs, accompanied by reduced concentrations of 5-HT, AChE, SP and VIP, coupled with an elevated concentration of NOS. However, ZZMRP treatment significantly improved these indicators. Furthermore, ZZMRP administration also significantly reversed the Lop-induced increase in apoptosis rate, ER stress symptoms, and the levels of proapoptotic and ER stress proteins while restoring lev-

els of antiapoptotic proteins. Moreover, the altered outcomes in apoptosis rate and protein levels involved in apoptosis were further reversed with the application of 4-PBA. Also, two decomposed recipes, DR1 and DR2, were also employed for the control experiments. TCMs in DR1 are primarily associated with regulating "qi" and enhancing intestinal motility, while those of DR2 are involved in regulating aqueous fluid and are associated with intestinal secretion. Consequently, DR1 significantly affected the level of NOS, VIP, and SP, whereas DR2 was closely associated with the level of 5-HT and AChE. Taken together, these results reveal that ZZMRP alleviates constipation through ER stress-mediated apoptosis in Lop-treated mice, suggesting its possible therapeutic efficacy.

Constipation is a common problem characterized by delayed expulsion of intestinal contents and slow colon peristalsis, which influences patients' quality of life and may cause various intestinal disorders. In the present study, the effect of ZZMRP, as well as its two decomposed recipes DR1 and DR2, on constipation was addressed. ZZMRP included the traditional Chinese medicines Zhishi, Baizhu, Huomaren, Baishao and Zi-wan, while DR1 contains Zhishi, Baizhu and Zi-wan, and DR2 comprises Huomaren and Baishao. The ingredients of ZZMRP were initially analysed and identified 14 key ingredients in ZZMRP, including Isosinensetin, isosakuranetin-7-O-rutinoside, Sinensetin, Naringenin, Nobiletin, Didymin, Arachidonic acid, Stigmasterol, Paeoniflorin, Kaempferol, (+)-catechin, Galangin, Isorhamnetin, and Quercetin, which matched with 44 active compounds based on the network pharmacology analysis [18]. This suggests the necessity for further experimental validation of these findings. Notably, isosinensetin and kaempferol were among the top 20 most prevalent components. Functionally, ZZMRP was considered to replenish qi and increase fluid and yin, correlating with its clinical application to promote intestinal motility and increase intestinal lumen moisture. DR1 primarily promotes intestinal motility, whereas DR2 increases intestinal lumen moisture. The differential ingredient analysis between ZZMRP and its decomposed recipes revealed involvement in several key signaling pathways. Differences between ZZMRP and DR1 affected the PI3K-Akt signaling pathway, mTOR signaling pathway, PPAR signaling pathway, FoxO signaling pathway, and cGMP-PKG signaling pathway, whereas differences between ZZMRP and DR2 were associated with FoxO signaling pathway, protein digestion and absorption, and nucleotide metabolism. Studies suggest that up-expression of the PI3K-Akt signaling pathway is found in lop-induced constipation [26] and interventions such as electroacupuncture have been reported to improve intestinal motility by suppressing this signaling in the colonic tissues of mice with functional constipation [27]. Additionally, PI3K/Akt/mTOR pathway is also involved in the improvement of methyltransferase-like 3 (METTL3) on slow transit constipation [28]. Yao and colleagues [29] revealed that pterostilbene improves Lop-induced intestinal motility disorder by suppressing oxidative stress-induced apoptosis of ICCs through the PI3K/AKT/Nrf2 signaling axis. Wang et al [30] reported that miR-129-3p regulates the autophagy of ICCs by targeting the AKT/mTOR signaling pathway in cases of slow transit constipation.

Several hallmarks characterize the Lop-induced constipation model, including reduced faecal pellets, faecal water content, and gastrointestinal transit ratio [31]. In this study, mice treated with Lop exhibited prolonged transit times and reduced ink progradation rate after the administration of charcoal meal, aligning with a previous study [24]. H&E staining revealed severe pathological changes in these mice. Additionally, decreased levels of ICCs were found in Lop-induced mice, accompanied by reduced concentrations of 5-HT, AChE, SP and VIP, as well as an elevated concentration of NOS. ICCs, mesenchymal cells critical to the gastrointestinal tract's motility, are essential in the pathogenesis of gastrointestinal motor diseases due to their role in mediating differentiation, proliferation, and functional responses through C-kit receptor activation [32]. Gastrointestinal hormones play a vital role in modulating gastrointestinal peristalsis under normal physiologic conditions. 5-HT promotes blood flow, electrolyte secretion and absorption, intestinal motility and perception of nausea or pain in the gastrointestinal tract [33]. AChE and SP show a strong effect of stimulating intestinal muscle contraction, enhancing peristalsis, whereas VIP exhibits a strong vasodilating and vasodilating effect, especially inhibiting the tone of the

intestinal muscles [34]. NOS typically inhibits intestinal contractions, contributing to constipation. However, treatment with Zhi Zhu Ma Ren pill (ZZMRP) effectively reversed these effects, improving constipation symptoms in Lop-induced mice.

The pathogenesis of constipation involves various mechanisms, among which apoptosis has been highlighted to play a crucial role. The results from our previous research exhibit that ICC apoptosis is prominently increased in colon tissue of Lop-treated rats, indicating that apoptosis has a role in constipation [35]. Similar results are also reported by other groups, and inhibition of apoptosis is an alternative strategy for the treatment of constipation [28, 36]. Previous research, including a study by Wang et al [37], demonstrated that Ji-Chuan decoction ameliorates slow transit constipation through modulation of intestinal glial cell apoptosis. Additionally, both pterostilbene, a natural polyphenol compound [29], and Xiao Chengqi formula [38] have been shown to improve constipation by inhibiting apoptosis. In the current study, ZZMRP introduction reversed the Lop-triggered elevation in the apoptosis rate, the relative protein expression of Bax, cleaved caspase-3 and cleaved PARP, along with mitigating the decrease in Bcl-2 levels. BCL-2 and Bax are key apoptotic regulators, with BCL-2 serving an antiapoptotic function and BAX a proapoptotic role [39]. Cleaved caspase-3, an active form of caspase 3, plays a pivotal role in different phases of the apoptotic pathway [40]. PARP, a Zn^{2+}-dependent DNA-binding protein, is crucial for DNA repair, recognizing and binding to DNA break ends. In the early stages of apoptosis, caspase-3 cleaves PARP into 2 fragments (89 kDa and 24 kDa), disabling its repair capacity. The 89 kDa fragment, in particular, exits the nucleus after production, serving as a marker for apoptosis [41]. Thus, ZZMRP reduced apoptosis in Lop-induced mice.

ER stress is another important mechanism of constipation, and its inhibition can improve the condition. For instance, Kim et al [22] demonstrated that spicatoside A in red Liriope platyphylla acts as a laxative in a constipation rat model by modulating mAChRs and ER stress signalling. Similarly, uridine has shown laxative effects through the inhibition of ER stress in loperamide-treated constipated SD rats [42]. ER stress typically activates major signalling pathways including ATF6, IRE1α, and PERK [43]. CHOP, initially identified as a molecule involved in ER stress-triggered apoptosis, shows markedly enhanced expression in response to ER stress by IRE1-, PERK- and ATF6-dependent transcriptional elicitation. The activation of ATF4, triggered by PERK-mediated phosphorylation of eIF2α, significantly contributes to CHOP induction in response to ER stress. In the present study, ZZMRP treatment effectively reversed Lop-induced enhancement in ER stress symptoms and relative protein levels of p-IRE1α/IRE1α, TRAF2, p-PERK/PERK, p-eIF2α/EIF2α, p-CHOP/CHOP, ATF6, and GRP78, thereby ameliorating ER stress in Lop-treated mice.

ER stress is characterized by the activation of the unfolded protein response (UPR), ER overload response, and caspase-12-mediated apoptosis. This condition can induce the expression of ER chaperones, such as glucose regulated protein 94 (GRP94) and calmodulin, which play protective roles and can autonomously trigger apoptosis. ER stress directly influences cellular fates, such as injury, adaptation or apoptosis, in response to stress. CHOP-deficient cells are resistant to ER stress-elicited apoptosis, underlining CHOP's crucial role in this process. Upregulation of CHOP has been revealed to induce cell cycle arrest and/or apoptosis [44]. Here, alterations in the apoptosis rates and the relative protein levels associated with apoptosis were reversed with the application of 4-PBA. Similar findings were also reported in the laxative effects of uridine through ER-mediated apoptosis in Lop-treated constipated SD rats [42]. Altogether, ZZMRP relieved apoptosis through ER stress in Lop-induced mice.

In conclusion, this study illustrated that ZZMRP relieved constipation from ER stress-mediated apoptosis in Lop-treated mice. However, a direct relationship between apoptosis and constipation was not definitively established due to funding limitations. Future research should explore this link further, possibly through using an inhibitor of apoptosis. Additionally, more preclinical and clinical trials are essential to confirm that ZZMRP may be an effective treatment for constipation.

Acknowledgements

We thank the support by the National Natural Science Foundation of China (grant nos. 82074429 and 82004173).

Disclosure of conflict of interest

None.

Address correspondence to: Dr. Xuegui Tang, Department of Integrated Traditional and Western Medicine Anorectal, Affiliated Hospital of North Sichuan Medical College, No. 63 Wenhua Road, Shunqing District, Nanchong 637000, Sichuan, China. Tel: +86-18989183808; E-mail: txg668nc@nsmc.edu.cn

References

[1] Bharucha AE. Constipation. Best Pract Res Clin Gastroenterol 2007; 21: 709-731.

[2] Forootan M, Bagheri N and Darvishi M. Chronic constipation: a review of literature. Medicine (Baltimore) 2018; 97: e10631.

[3] Werth BL, Williams KA, Fisher MJ and Pont LG. Defining constipation to estimate its prevalence in the community: results from a national survey. BMC Gastroenterol 2019; 19: 75.

[4] Staller K, Barshop K, Kuo B and Ananthakrishnan AN. Depression but not symptom severity is associated with work and school absenteeism in refractory chronic constipation. J Clin Gastroenterol 2018; 52: 407-412.

[5] Lindberg G, Hamid SS, Malfertheiner P, Thomsen OO, Fernandez LB, Garisch J, Thomson A, Goh KL, Tandon R, Fedail S, Wong BC, Khan AG, Krabshuis JH and LeMair A; World Gastroenterology Organisation. World Gastroenterology Organisation global guideline: constipation--a global perspective. J Clin Gastroenterol 2011; 45: 483-487.

[6] Ikarashi N, Baba K, Ushiki T, Kon R, Mimura A, Toda T, Ishii M, Ochiai W and Sugiyama K. The laxative effect of bisacodyl is attributable to decreased aquaporin-3 expression in the colon induced by increased PGE2 secretion from macrophages. Am J Physiol Gastrointest Liver Physiol 2011; 301: G887-895.

[7] Patcharatrakul T, Valestin J, Schmeltz A, Schulze K and Rao SSC. Factors associated with response to biofeedback therapy for dyssynergic defecation. Clin Gastroenterol Hepatol 2018; 16: 715-721.

[8] Shen L, Huang C, Lu X, Xu X, Jiang Z and Zhu C. Lower dietary fibre intake, but not total water consumption, is associated with constipation: a population-based analysis. J Hum Nutr Diet 2019; 32: 422-431.

[9] Gasior A, Reck C, Vilanova-Sanchez A, Diefenbach KA, Yacob D, Lu P, Vaz K, Di Lorenzo C, Levitt MA and Wood RJ. Surgical management of functional constipation: an intermediate report of a new approach using a laparoscopic sigmoid resection combined with malone appendicostomy. J Pediatr Surg 2018; 53: 1160-1162.

[10] Chen JQ, Chen YY, Tao HJ, Pu ZJ, Shi XQ, Zhang J, Tan YJ, Yue SJ, Zhou GS, Shang EX, Tang YP and Duan JA. An integrated metabolomics strategy to reveal dose-effect relationship and therapeutic mechanisms of different efficacy of rhubarb in constipation rats. J Pharm Biomed Anal 2020; 177: 112837.

[11] Zhao X, Fang Y, Ye J, Qin F, Lu W and Gong H. A meta-analysis of randomized controlled trials of a traditional Chinese medicine prescription, modified RunChang-Tang, in treating functional constipation. Medicine (Baltimore) 2021; 100: e25760.

[12] Chen YY, Cao YJ, Tang YP, Yue SJ and Duan JA. Comparative pharmacodynamic, pharmacokinetic and tissue distribution of Dahuang-Gancao decoction in normal and experimental constipation mice. Chin J Nat Med 2019; 17: 871-880.

[13] Wang LF, Liu XL, Li HT, Chen QY, Wang Y, Zou B, Yang M, Zhang XF and Wang F. Mechanism of Aurantii Fructus Immaturus volatile oil in treatment of slow transit constipation based on network pharmacology. Zhongguo Zhong Yao Za Zhi 2020; 45: 1909-1917.

[14] Yan S, Hao M, Yang H, Sun M, Wu B, Yue Y and Wang X. Metabolomics study on the therapeutic effect of the Chinese herb pair Fructus Aurantii Immaturus and Rhizoma Atractylodis Macrocephalae in constipated rats based on UPLC-Q/TOF-MS analysis. Ann Palliat Med 2020; 9: 2837-2852.

[15] Gao L, Wang J, Li F, Deng Y and Gao S. Literature-based analysis on relationship of symptoms, drugs and therapies in treatment of intestinal diseases. J Tradit Chin Med 2014; 34: 106-114.

[16] Tsai JC, Tsai S and Chang WC. Effect of ethanol extracts of three Chinese medicinal plants with laxative properties on ion transport of the rat intestinal epithelia. Biol Pharm Bull 2004; 27: 162-165.

[17] Liu G, Wang Z, Li X, Liu R, Li B, Huang L, Chen Y, Zhang C, Zhang H, Li Y, Chen Y, Yin H and Fang W. Total glucosides of paeony (TGP) alleviates constipation and intestinal inflammation in mice induced by Sjögren's syndrome. J Ethnopharmacol 2020; 260: 113056.

[18] Wen Y, Zhan Y, Tang S, Kang J, Wu R and Tang X. Mechanistic prediction of Chinese herb compound (Zhi Zhu Ma Ren Pill) in the treatment of constipation using network pharma-

cology and molecular docking. Nat Prod Commun 2022; 17: 1934578X221124780.
[19] Zheng H, Liu YJ, Chen ZC and Fan GQ. miR-222 regulates cell growth, apoptosis, and autophagy of interstitial cells of Cajal isolated from slow transit constipation rats by targeting c-kit. Indian J Gastroenterol 2021; 40: 198-208.
[20] Gardner BM and Walter P. Unfolded proteins are Ire1-activating ligands that directly induce the unfolded protein response. Science 2011; 333: 1891-1894.
[21] Kim JE, Park JJ, Lee MR, Choi JY, Song BR, Park JW, Kang MJ, Son HJ, Hong JT and Hwang DY. Constipation in Tg2576 mice model for Alzheimer's disease associated with dysregulation of mechanism involving the mAChR signaling pathway and ER stress response. PLoS One 2019; 14: e0215205.
[22] Kim JE, Go J, Lee HS, Hong JT and Hwang DY. Spicatoside A in red Liriope platyphylla displays a laxative effect in a constipation rat model via regulating mAChRs and ER stress signaling. Int J Mol Med 2019; 43: 185-198.
[23] He Q, Han C, Huang L, Yang H, Hu J, Chen H, Dou R, Ren D and Lin H. Astragaloside IV alleviates mouse slow transit constipation by modulating gut microbiota profile and promoting butyric acid generation. J Cell Mol Med 2020; 24: 9349-9361.
[24] Zhan Y, Wen Y, Du LJ, Wang XX, Tang SY, Kong PF, Huang WG and Tang XG. Effects of maren pills on the intestinal microflora and short-chain fatty acid profile in drug-induced slow transit constipation model rats. Front Pharmacol 2022; 13: 804723.
[25] Tan X, Cai D, Chen N, Du S, Qiao D, Yue X, Wang T, Li J, Xie W and Wang H. Methamphetamine mediates apoptosis of vascular smooth muscle cells via the chop-related endoplasmic reticulum stress pathway. Toxicol Lett 2021; 350: 98-110.
[26] Choi YJ, Kim JE, Lee SJ, Gong JE, Jang M, Hong JT and Hwang DY. Loperamide-induced constipation activates inflammatory signaling pathways in the mid colon of SD rats via complement C3 and its receptors. Curr Mol Med 2022; 22: 458-469.
[27] Wang L, Chen Y, Xu MM, Cao W, Zheng QH, Zhou SY, Yao JP, Xi MH, Qin HY, Li Y and Zhang W. Electroacupuncture alleviates functional constipation in mice by activating enteric glial cell autophagy via PI3K/AKT/mTOR signaling. Chin J Integr Med 2023; 29: 459-469.
[28] Gong WJ, Li R, Dai QQ and Yu P. METTL3 contributes to slow transit constipation by regulating miR-30b-5p/PIK3R2/Akt/mTOR signaling cascade through DGCR8. J Gastroenterol Hepatol 2022; 37: 2229-2242.
[29] Yao Z, Fu S, Ren B, Ma L and Sun D. Based on network pharmacology and gut microbiota analysis to investigate the mechanism of the laxative effect of pterostilbene on loperamide-induced slow transit constipation in mice. Front Pharmacol 2022; 13: 913420.
[30] Wang H, Ren B, Pan J, Fu S, Liu C and Sun D. Effect of miR-129-3p on autophagy of interstitial cells of Cajal in slow transit constipation through SCF C-kit signaling pathway. Acta Biochim Pol 2022; 69: 579-586.
[31] Liu W and Zhi A. The potential of Quercetin to protect against loperamide-induced constipation in rats. Food Sci Nutr 2021; 9: 3297-3307.
[32] Lorincz A, Redelman D, Horváth VJ, Bardsley MR, Chen H and Ordög T. Progenitors of interstitial cells of cajal in the postnatal murine stomach. Gastroenterology 2008; 134: 1083-1093.
[33] Manzella C, Singhal M, Alrefai WA, Saksena S, Dudeja PK and Gill RK. Serotonin is an endogenous regulator of intestinal CYP1A1 via AhR. Sci Rep 2018; 8: 6103.
[34] Gan Y, Liang J, Diao W, Zhou X, Mu J, Pang L, Tan F and Zhao X. Lactobacillus plantarum KSFY06 and geniposide counteract montmorillonite-induced constipation in Kunming mice. Food Sci Nutr 2020; 8: 5128-5137.
[35] Wu R, Zhang Z, Xu Q, Liu F, Zhan Y, Wang Q, Du L and Tang X. Integration of network pharmacology and experimental verifications reveals the Bian-Se-Tong mixture can alleviate constipation in STC rats by reducing apoptosis of Cajal cells via activating PI3K-Akt signaling pathway. Heliyon 2024; 10: e28022.
[36] Zhou Q, He Z, Yan S, Wang X and Wu B. Nobiletin, an active component of Wenyang Yiqi formula, alleviates constipation associated depression through targeting MAPT to inhibit the MAPK signaling pathway. Phytomedicine 2024; 126: 155203.
[37] Wang XM, Lv LX, Qin YS, Zhang YZ, Yang N, Wu S, Xia XW, Yang H, Xu H, Liu Y and Ding WJ. Ji-Chuan decoction ameliorates slow transit constipation via regulation of intestinal glial cell apoptosis. World J Gastroenterol 2022; 28: 5007-5022.
[38] Zhou Q, Zhang D, Zhang H, Wan X, Hu B, Zou Q, Su D, Peng H, Huang D and Ren D. Effects of Xiao Chengqi Formula on slow transit constipation by assessing gut microbiota and metabolomics analysis in vitro and in vivo. Front Pharmacol 2022; 13: 864598.
[39] Edlich F. BCL-2 proteins and apoptosis: recent insights and unknowns. Biochem Biophys Res Commun 2018; 500: 26-34.
[40] Asadi M, Taghizadeh S, Kaviani E, Vakili O, Taheri-Anganeh M, Tahamtan M and Savardashtaki A. Caspase-3: structure, function,

and biotechnological aspects. Biotechnol Appl Biochem 2022; 69: 1633-1645.
[41] Peng X, Pan W, Jiang F, Chen W, Qi Z, Peng W and Chen J. Selective PARP1 inhibitors, PARP1-based dual-target inhibitors, PROTAC PARP1 degraders, and prodrugs of PARP1 inhibitors for cancer therapy. Pharmacol Res 2022; 186: 106529.
[42] Kim JE, Song BR, Yun WB, Choi JY, Park JJ, Lee MR and Hwang DY. Correlation between laxative effects of uridine and suppression of ER stress in loperamide induced constipated SD rats. Lab Anim Res 2017; 33: 298-307.
[43] Chen X, Shi C, He M, Xiong S and Xia X. Endoplasmic reticulum stress: molecular mechanism and therapeutic targets. Signal Transduct Target Ther 2023; 8: 352.
[44] Li Y, Guo Y, Tang J, Jiang J and Chen Z. New insights into the roles of CHOP-induced apoptosis in ER stress. Acta Biochim Biophys Sin (Shanghai) 2014; 46: 629-640.

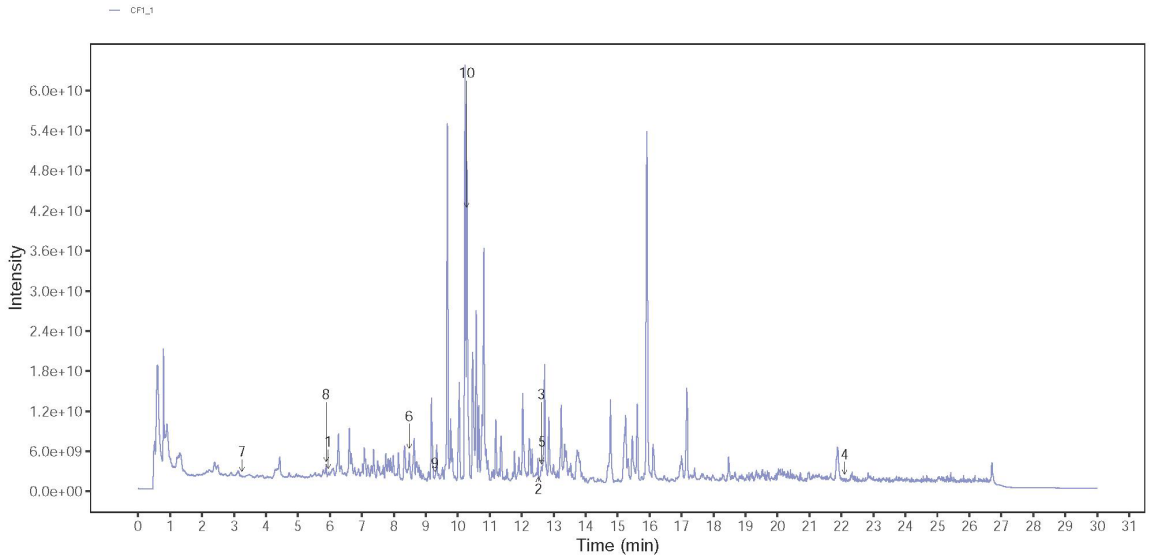

Figure S1. Positive ingredients of DR1.

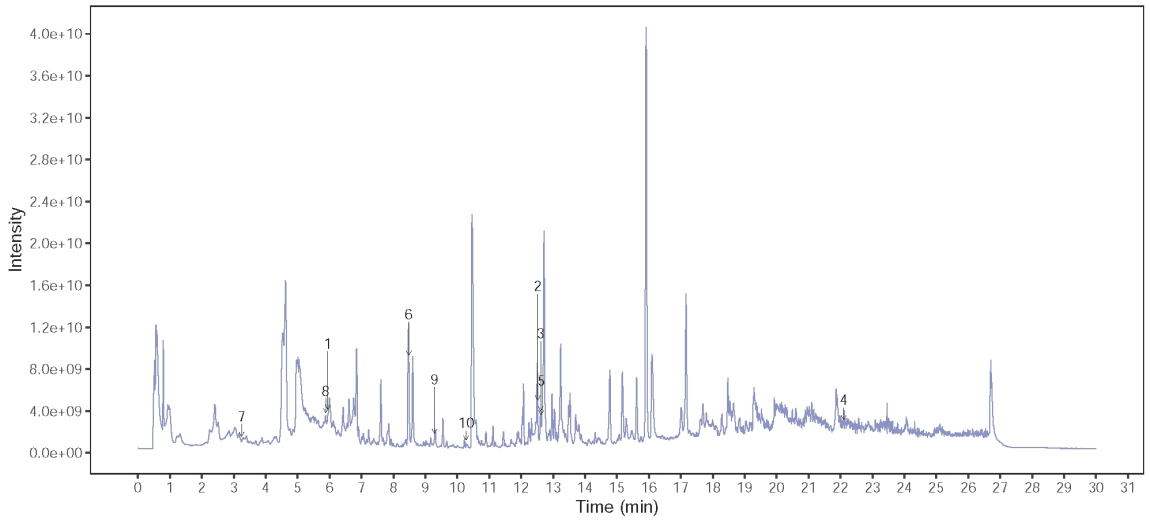

Figure S2. Positive ingredients of DR2.

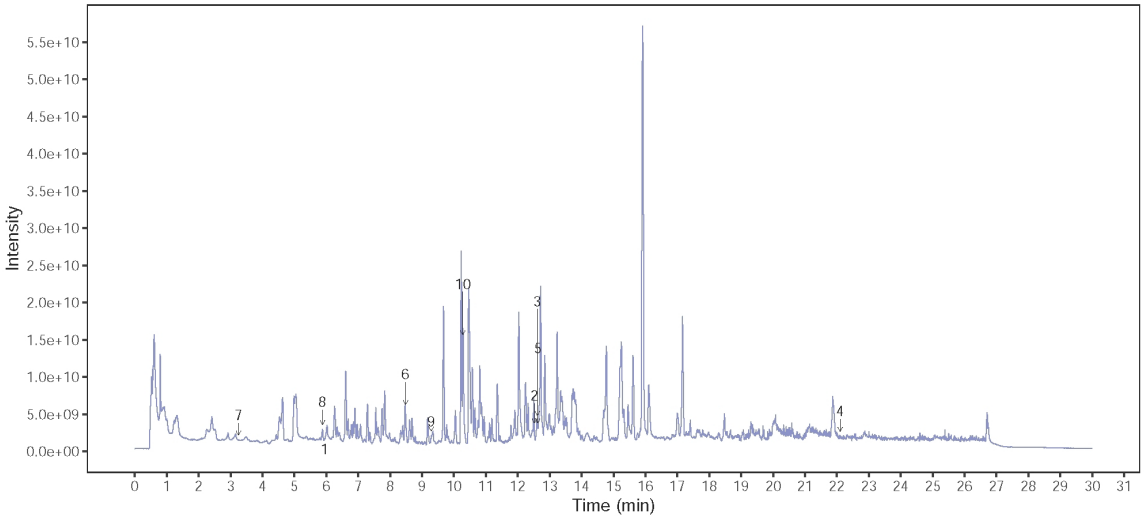

Figure S3. Positive ingredients of ZZMRP.

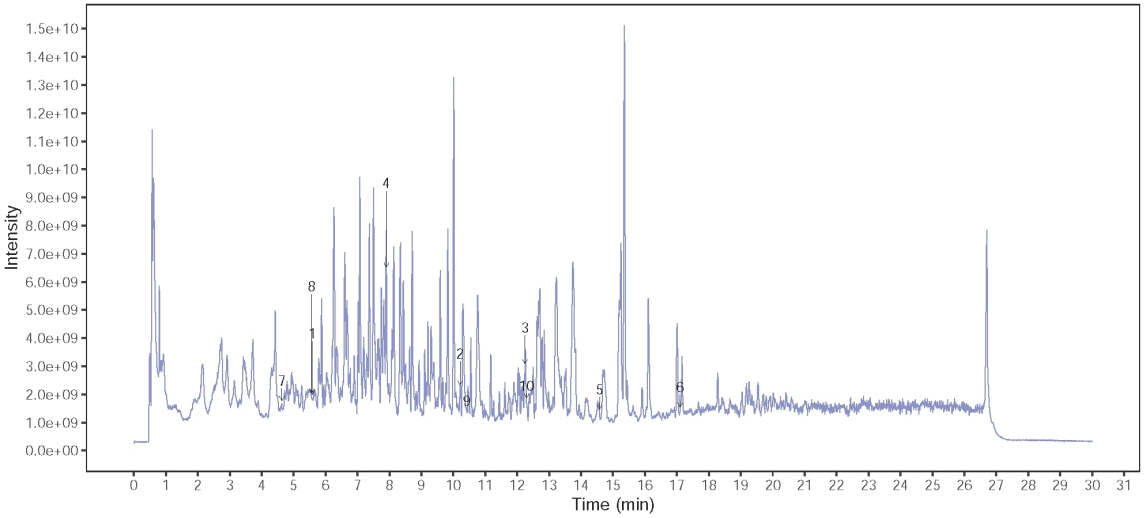

Figure S4. Negative ingredients of DR1.

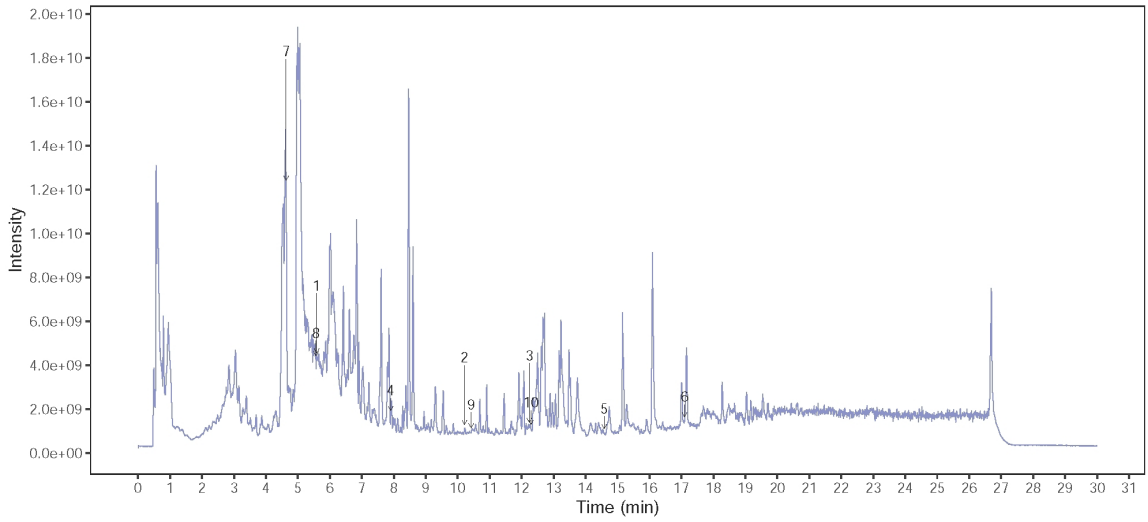

Figure S5. Negative ingredients of DR2.

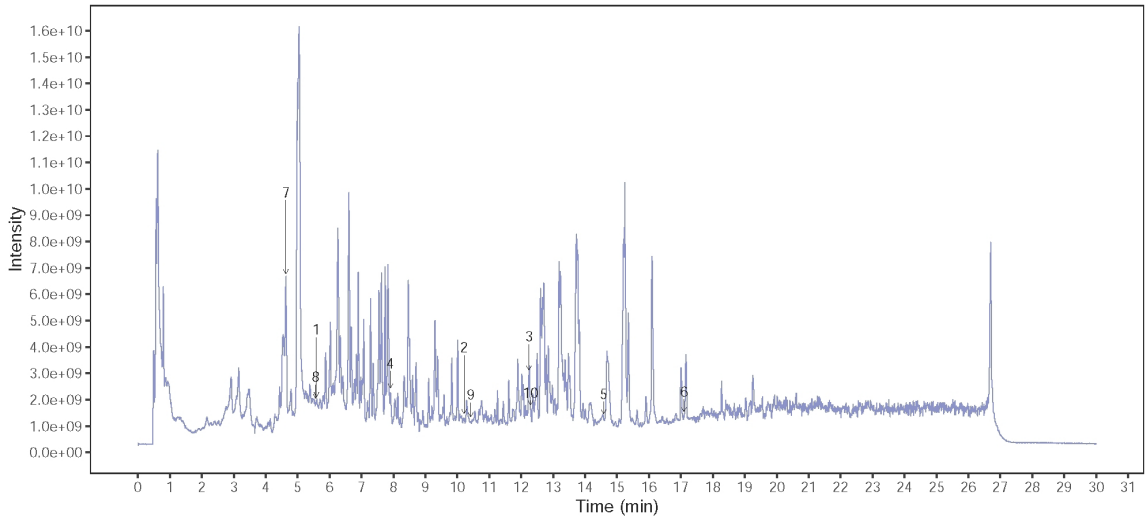

Figure S6. Positive ingredients of ZZMRP.

Table S1. The top 20 ingredients of DR1 DR2 and ZZMRP

DR1	DR2	ZZMRP
Hexamethylquercetagetin	"[(1S,2S,3R,5R,6S,8S)-6-hydroxy-8-methyl-3-{[(2S,3R,4S,5S,6R)-3,4,5-trihydroxy-6-(hydroxymethyl)oxan-2-yl]oxy}-9,10-dioxatetracyclo[4.3.1.02]decan-2-yl]methyl benzoate"	Hexamethylquercetagetin
Atractylenolide I	Eriodictryol 7-O-glucoside	Atractylenolide I
LPC 16:0	LPC 16:0	"[(1S,2S,3R,5R,6S,8S)-6-hydroxy-8-methyl-3-{[(2S,3R,4S,5S,6R)-3,4,5-trihydroxy-6-(hydroxymethyl)oxan-2-yl]oxy}-9,10-dioxatetracyclo[4.3.1.02]decan-2-yl]methyl benzoate"
1-Aminocyclohexanecarboxylic acid	Asarylaldehyde	LPC 16:0
Isosinensetin	Citric acid	Pterolactam
Curzerene	Erucamide	1-Aminocyclohexanecarboxylic acid
(+)-Nootkatone	(+)-Catechin hydrate	Isosinensetin
Pterolactam	2-Hydroxy-3-(4-methoxyphenyl)propanoic acid	L-Malic acid
"2,3-Dihydro-6-methyl-1H-pyrrolizine-5-carboxaldehyde"	FA 18:1+10	(+)-Nootkatone
6-Demethoxytangeretin	LINOLEATE	Citric acid
"5,7-dihydroxy-2-(4-hydroxyphenyl)-6,8-bis[3,4,5-trihydroxy-6-(hydroxymethyl)oxan-2-yl]chromen-4-one"	Pterolactam	Dicaffeoyl quinic acid
Dehydrophytosphingosine	Trigonelline HCl	"17,18-Dichloro-3,13-diethyl-6-(hydroxymethyl)-9-phenyldodecahydropyrrolo[1,2-d][1,4,7,10,13]pentaazacyclohexadecine-1,4,7,11,14(8H)-pentone"
Naringenin-7-O-rutinoside	Choline chloride	Naringenin-7-O-rutinoside
Citric acid	Arginine	Erucamide
L-Malic acid	"12,13-EODE"	"2,3-Dihydro-6-methyl-1H-pyrrolizine-5-carboxaldehyde"
Naringin	D-Gluconic acid	2-({3-Phenyl-3-[(N-{2-[(1H-pyrrol-2-ylcarbonyl)amino]butanoyl}seryl)amino]propanoyl}amino)butanoic acid
Erucamide	Pyrogallol	Arginine
Arginine	"3,5-Dimethyl-2-propylpyrazine"	6-Demethoxytangeretin
Dicaffeoyl quinic acid	"3,4-Dihydroxymandelic acid"	"5,7-dihydroxy-2-(4-hydroxyphenyl)-6,8-bis[3,4,5-trihydroxy-6-(hydroxymethyl)oxan-2-yl]chromen-4-one"
N-Methyltyramine	8-Desoxygartanin	Kaempferol